Structural, transport, magnetic properties and Raman spectroscopy of orthorhombic $Y_{1-x}Ca_xMnO_3$ ($0 \leq x \leq 0.5$)

M. N. Iliev[1], B. Lorenz[1], A. P. Litvinchuk[1], Y.-Q. Wang[1], Y. Y. Sun[1], C. W. Chu[1,2,3]

[1] *Texas Center for Superconductivity and Advanced Materials and Department of Physics, University of Houston, Houston, Texas 77204-5002*

[2] *Lawrence Berkeley National Laboratory, Cyclotron Road, Berkeley, CA 94720*

[3] *Hong Kong University of Science and Technology, Hong Kong, China*

(Dated: February 2, 2008)

Abstract

Orthorhombic $Y_{1-x}Ca_xMnO_3$ ($0 \leq x \leq 0.5$) was prepared under high pressure and the variations with x of its structural, magnetic, electrical properties and the polarized Raman spectra were investigated. The lattice parameters change systematically with x. Although there are strong indications for increasing disorder above $x = 0.20$, the average structure remains orthorhombic in the whole substitutional range. Ca doping increases conductivity, but temperature dependence of resistivity ρ(T) remains semiconducting for all x. The average magnetic exchange interaction changes from antiferromagnetic for $x < 0.08$ to ferromagnetic for $x > 0.08$. The evolution with x of the Raman spectra provides evidence for increasingly disordered oxygen sublattice at $x \geq 0.10$, presumably due to quasistatic and/or dynamical Jahn-Teller distortions.

PACS numbers: 75.47.Lx,75.30.-m,61.10.Nz,78.30.-j

I. INTRODUCTION

At atmospheric pressure $Y_{1-x}Ca_xMnO_3$ ($0 \leq x < 0.25$), similarly to the rare-earth manganites RMnO$_3$, for R with smaller ionic radius (R = Ho, Er, Tm, Yb, Lu) crystallizes in the hexagonal $P6_3cm$ structure whereas the orthorhombic, distorted perovskite structure is the stable phase for $Y_{1-x}Ca_xMnO_3$ with $x \geq 0.25$.[1] Upon annealing under high pressure, some hexagonal manganites, such as YMnO$_3$ and HoMnO$_3$, can be converted to their orthorhombic $Pnma$ phase.[2] The Ca- and Sr-doped orthorhombic rare-earth manganites have been a subject of intensive studies since the phenomenon "colossal magnetoresistance"(CMR) has been rediscovered.[3] To our knowledge, there are however no reports on the synthesis and properties of doped yttrium-based orthorhombic manganites for $x < 0.25$. The $Y_{1-x}Ca_xMnO_3$ orthorhombic system is of particular interest as it could be compared to the model $La_{1-x}Ca_xMnO_3$ system, where Ca doping and conversion of part of the Jahn-Teller Mn^{3+} ions in non-Jahn-Teller Mn^{4+} ions results in a complex magnetic phase diagram and strong interplay between structural, magnetic and transport properties.

In this work we report the synthesis of orthorhombic series $Y_{1-x}Ca_xMnO_3$ and first results on the variations with x of structural parameters, resistivity, magnetic properties and Raman spectra over the doping range $0 \leq x \leq 0.5$. The lattice parameters change systematically with x. Although there are strong indications for increasing disorder above $x = 0.20$, the average structure remains orthorhombic in the whole substitutional range. Ca doping increases conductivity, but the temperature dependence of the resistivity ρ(T) remains semiconducting for all x. It was found, however, that the average magnetic exchange interaction changes from antiferromagnetic for $x < 0.08$ to ferromagnetic for $x > 0.08$. The evolution with x of the Raman spectra provide strong indications for increasingly disordered oxygen sublattice at $x \geq 0.10$, presumably due to quasistatic and/or dynamical Jahn-Teller distortions.

II. SAMPLES AND EXPERIMENT

As a first step in samples preparation, ceramic pellets of hexagonal $Y_{1-x}Ca_xMnO_3$ (x = 0.00, 0.03, 0.06, 0.10 and 0.20) and orthorhombic $Y_{1-x}Ca_xMnO_3$ (x = 0.30 and 0.50) were synthesized by solid state reaction. The prescribed amounts of Y_2O_3, $CaCO_3$, and Mn_2O_3

were mixed and preheated at 900 to 1000° C in oxygen for 16 hours followed by sintering at 1140 to 1170°C for one day under oxygen atmosphere. The hexagonal samples were resintered in a high pressure furnace under 35 kbar at 1015 to 1030 °C for 5 h. Under these conditions the hexagonal phase was completely transformed into the metastable orthorhombic structure. The x-ray-diffraction (XRD) pattern were collected at room temperature using a Rigaku DMaxIII/B x-ray diffractometer.

Magnetization measurements were conducted employing the MPMS SQUID magnetometer (Quantum Design) at an external field of 500 Oe. The dc resistivity was measured by the standard four-probe method using a Keithley 220 current source and a Keithley 182 nanovoltmeter. The Raman spectra were obtained at room temperature using a HR640 spectrometer equipped with microscope, notch filters and liquid-nitrogen-cooled CCD detector. 514.5 nm and 632.8 laser lines, focused with an $\times 100$ objective on the sample's surface in a spot of (2-3 μm) diameter, were used for excitation. For the most samples the size of the the microcrystals constituting the pellet was larger than the laser spot, which made it possible to select microcrystals with proper orientation of crystallographic axes with respect to incident polarization and obtain polarized spectra in nearly exact scattering configurations.

III. RESULTS AND DISCUSSION

A. Structural, Electric and Magnetic Measurements

The x-ray spectra of $Y_{1-x}Ca_xMnO_3$ are shown in Fig.1 for $x = 0$ to $x = 0.5$. All reflections can be indexed within the orthorhombic symmetry, space group $Pnma$. The absence of impurity lines proves the high phase purity and the success of the high-pressure synthesis in stabilizing the $Pnma$ structure for the Ca content between 0 and 0.5. A remarkable broadening of the x-ray lines is observed above $x = 0.2$ that indicates an increased disorder of the cations at higher substitution, x. The lattice constants change systematically with x, as shown in Fig.2. The largest change is the decrease of a by up to 7% at $x = 0.5$. In contrast, the c-axis is almost not affected by the Ca doping. The b-axis shows a distinct, but moderate increase from $x = 0$ to $x = 0.5$, the total change being no more than 1.5%. The systematic change of the lattice constants with x and the absence of impurity lines

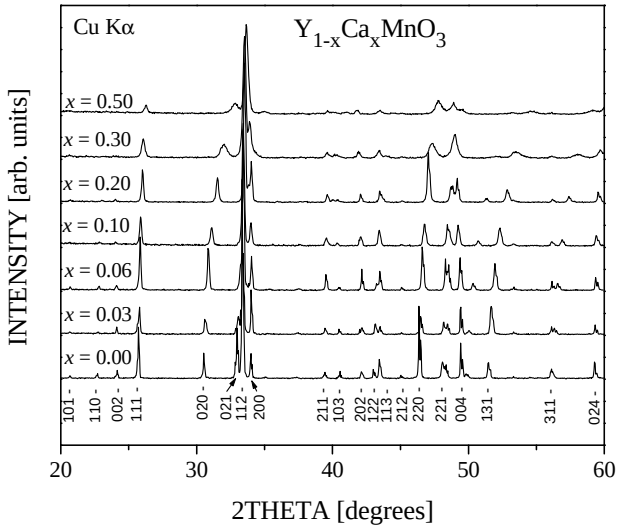

FIG. 1: X-ray diffraction pattern of $Y_{1-x}Ca_xMnO_3$ ($0 \leq x \leq 0.5$.)

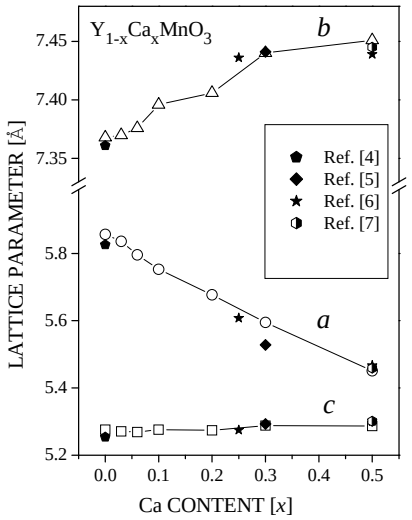

FIG. 2: Variation of the lattice parameters of $Y_{1-x}Ca_xMnO_3$ with x

in the x-ray spectra unambiguously prove that the Ca ions in fact replace the Y ions in the perovskite-like structure of $Y_{1-x}Ca_xMnO_3$. Our values of the lattice parameters are in good agreement with data of recent publications for $x = 0$, $x = 0.25$, $x = 0.3$, and $x = 0.5$ (included in Fig.2 as symbols).[4, 5, 6, 7] Recent neutron powder diffraction (NPD) experiments[8] estimated a considerably longer a-axis (5.97 Å as compared with 5.857 Å of the present investigation). The discrepancy is probably due to the excess oxygen reported for the NPD samples.

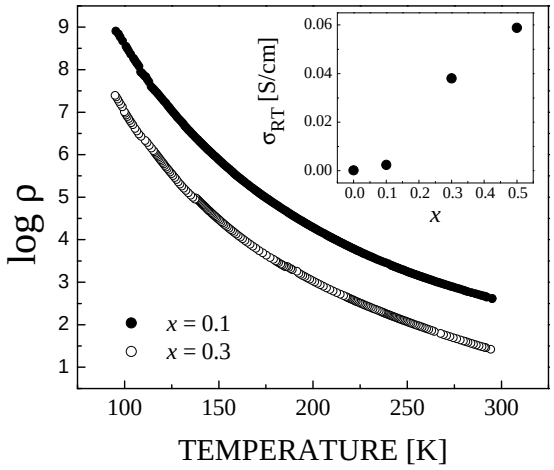

FIG. 3: Resistivity of $Y_{1-x}Ca_xMnO_3$ as function of temperature (for $x = 0.1$ and $x = 0.3$). Inset: Room temperature conductivity as function of x.

The doping of orthorhombic $YMnO_3$ with Ca introduces charge carriers by removing one electron per Ca from the Mn^{3+} ions. The resulting Mn^{4+} "carries" one hole that can hop among the Mn-ions via the hybridization of Mn d-states with the oxygen p-states. The conductivity of the doped compound should increase with x. In fact, the room temperature conductivity of ortho-$YMnO_3$ increases by a factor of about 300 between $x = 0$ and $x = 0.5$ (see the inset of Fig. 3). The characteristic temperature dependence of the resistivity, ρ(T), is semiconducting for all $x < 0.5$. Fig.3 (main panel) shows two typical examples of ρ(T) for $x = 0.1$ and $x = 0.3$.

The magnetic properties of the series $Y_{1-x}Ca_xMnO_3$ are summarized in Fig.4. For $x = 0$ the inverse magnetic susceptibility exhibits a Curie-Weiss-like linear temperature dependence at T $>$ 80 K and a sharp anomaly at the antiferromagnetic transition temperature, $T_N = 42.5$ K. From the high-temperature data the paramagnetic Curie temperature and the effective magnetic moment per Mn ion are estimated as $\Theta = -54.7$ K and $\mu_{eff} = 5.05\ \mu_B$, respectively. The effective moment is close to the value of 4.9 μ_B for the free Mn^{3+} ion (spin only, S=2). The values for Θ and μ_{eff} are in good agreement with those reported in Ref.[9](-67 K, 4.98μ_B), but deviate significantly from the recent results (-26 K, 3.69μ_B) of Ref.[8]. We attribute the latter discrepancy to the presence of a significant amount of hexagonal $YMnO_3$ and excess oxygen in the samples of Ref.[8]. The high-pressure synthesized specimens used in the present investigation are of high phase purity. The clear decrease

of the magnetic susceptibility below T_N is a further indication that the composition of the compound is close to stoichiometric. Deviations from stoichiometry (e.g. excess oxygen) will result in the presence of Mn^{4+} ions with a paramagnetic contribution to the susceptibility that can easily be detected below T_N.

The doping of ortho-$YMnO_3$ with Ca^{2+} results in a change of magnetic properties. Up to $x = 0.3$ the high-temperature susceptibility still exhibits Curie-Weiss behavior (Fig. 4). With increasing x the effective moment changes very little but Θ increases rapidly from -55 K ($x = 0$) to +63 K at $x = 0.3$. Fig. 5 shows Θ as function of x. The paramagnetic Curie temperature crosses zero close to 8% of Ca doping. The change of sign of Θ indicates a change of the average magnetic exchange interaction from antiferromagnetic (AFM, $x < 0.08$) to ferromagnetic (FM, $x > 0.08$), as illustrated in Fig. 5. This change is a consequence of the presence of Mn^{4+} ions for $x > 0$. For $x = 0$ the magnetic exchange of two neighboring Mn^{3+} is mediated by the oxygen ions between them and is ascribed to the superexchange mechanism with a resulting AFM coupling of the moments. With Ca doping Mn^{4+} ions are created. These Mn^{4+} ions do not participate in the superexchange interaction but open the double exchange interaction channel whenever they are next to an Mn^{3+}. The double exchange is ferromagnetic in its nature because of a gain in kinetic energy (the hole at the Mn^{4+} can hop to the neighboring Mn^{3+}) if the magnetic moments of both Mn-ions are parallel. This explains the gradual crossover of the paramagnetic Curie temperature from negative to positive values with increasing x as estimated from the high-T susceptibility data. Note that Θ obtained from the data shown in Fig.5 is an effective quantity, characteristic for the average response to field and temperature of all Mn moments, those coupled by AFM superexchange as well as those coupled by FM double exchange interactions to their respective neighbors. Our data clearly demonstrate that Ca doping of orthorhombic $YMnO_3$ is a powerful tool to tune the spin correlations from AFM superexchange to predominatly FM double exchange correlations. However, the increasing FM spin coupling does not introduce ferromagnetic lang range order down to the lowest temperatures in agreement with recent results for x=0.3.[6] The low temperature AFM Neel transition of ortho-$YMnO_3$ is also affected by the Ca doping. The relative enhancement of the magnetic susceptibility below T_N for $x > 0$ (as compared to $x = 0$) is an indication of the presence of Mn^{4+} ions and their paramagnetic contribution to the spin susceptibility. The Neel temperature decreases with increasing x due to a gradual reduction of the AFM superexchange correlations (Fig.

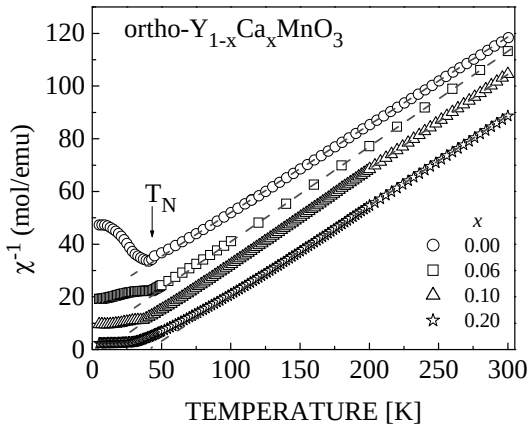

FIG. 4: Inverse magnetic susceptibility of orthorhombic $Y_{1-x}Ca_xMnO_3$ for $x = 0$ to $x = 0.2$.

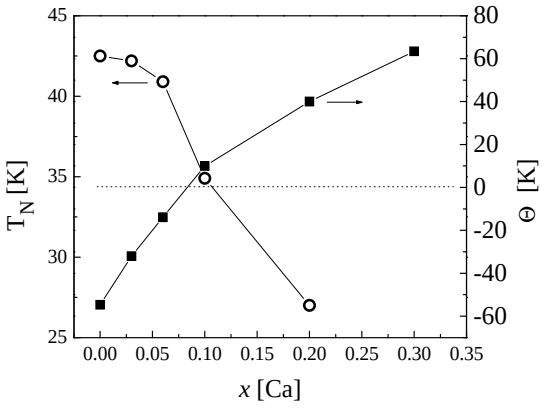

FIG. 5: Effective paramagnetic Curie temperature of orthorhombic $Y_{1-x}Ca_xMnO_3$ estimated from the high-temperature magnetic susceptibility (filled squares, right scale) and the Neel temperature for the AFM transition (open circles, left scale).

5). The AFM transition is sharp up to $x = 0.2$, but it broadens at higher doping levels. Only data for T_N up to $x = 0.2$ have therefore been included in the figure. The broadening of the magnetic transition above $x = 0.2$ is consistent with the observed broadening of the x-ray reflections and the Raman bands (see next Section)) and with the model of short range ferromagnetism and a spin glass state proposed recently for x=0.3.[6] It indicates the increasing influence of disorder on the physical properties of ortho-$Y_{1-x}Ca_xMnO_3$.

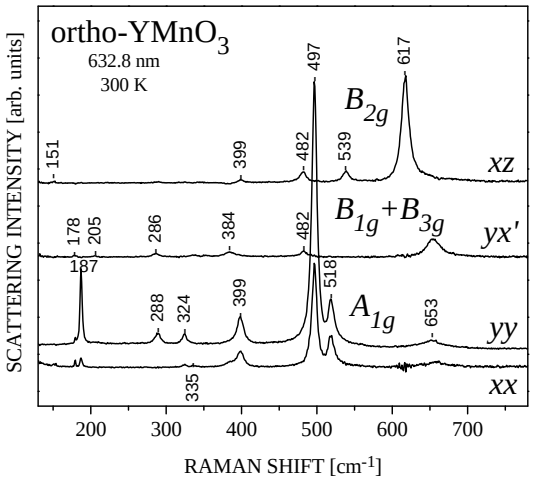

FIG. 6: Polarized Raman spectra of $YMnO_3$. The assignment of Raman lines to particular atomic motions is given in Ref.[10].

B. Raman Spectra

The polarized Raman spectra of undoped $YMnO_3$, shown in Fig.6, are identical to those reported in Ref.[10], where an assignment of the lines to particular phonon modes has been done too. The variations with x of the spectra of $Y_{1-x}Ca_xMnO_3$, measured with parallel (HH) and crossed (HV) scattering configurations, are shown in Fig.7. The HH configuration is close to xx and the Raman lines correspond to modes of A_g symmetry. The modes allowed with the HV (nearly xz) configuration are of B_{2g} symmetry.

As it follows from Fig.7, within the doping range $0 \leq x \leq 0.10$ the line widths moderately increase with x, but their position and relative intensity remain practically unchanged. At $x = 0.10$ there is a visible increase in intensity of the high frequency HH band at 644 cm^{-1} and the HV band at 654 cm^{-1}. For $x = 0.20$ these bands broaden, increase further in intensity and shift towards lower wavenumbers along with the bands originating from the 496 $cm^{-1}(A_g)$ and 617 $cm^{-1}(B_{2g})$ lines. At $x = 0.30$ the overall intensity of the spectra is reduced. The HV spectrum consists of only two broad bands centered at 495 cm^{-1} and 624 cm^{-1}. Except for broad bands close to these positions, the corresponding HH spectrum contains two additional weak bands at lower wavenumbers. The evolution of the HV spectrum between $x = 0.10$ and $x = 0.30$ is given in more detail in Fig.8. No Raman bands of detectable intensity are observed for $x = 0.5$.

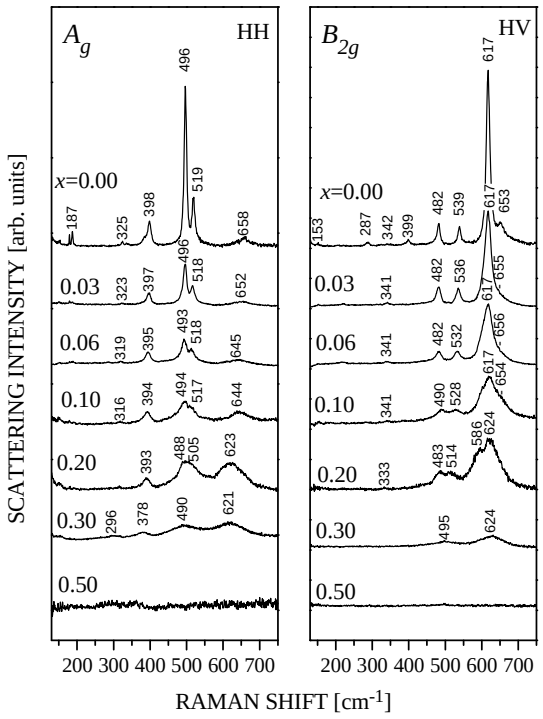

FIG. 7: Variations with x of the Raman spectra of $Y_{1-x}Ca_xMnO_3$. The HH and HV configurations are close, respectively to xx and xz

The Raman spectra for $x \geq 0.10$ are similar to those reported earlier for other $R^{3+}_{1-x}A^{2+}_{x}MnO_3$ (R = rare earth, A = Ca,Sr,Ba; $x \geq 0.1$) systems, [11, 12, 13, 14, 15, 16, 17] where 2 or 3 broad bands are observed at positions close to those of the strongest lines for nominally undoped $RMnO_3$. On the basis of this closeness, the broad bands have usually been assigned to the corresponding Raman allowed modes in the parent *Pnma* structure.

An alternative explanation for the broad band origin has recently been proposed by Iliev et al.[18]. It has been argued that at higher doping levels the spectral profiles reflect smeared partial phonon density-of-states (PDOS) related to oxygen vibrations rather than broadened Γ-point Raman allowed phonon modes. Indeed, the coexistence in doped manganites of Jahn-Teller-distorted ($Mn^{3+}O_6$) and undistorted ($Mn^{4+}O_6$) octahedra and the $Mn^{3+} \leftrightarrows Mn^{4+}$ charge transfer results in strong quasistatic or/and dynamical Jahn-Teller disorder of the oxygen sublattice. The loss of translational symmetry activates otherwise Raman forbidden oxygen vibrations, corresponding to the off-center phonon modes in ordered parent compound. In support of this model are: (i) the good correspondence between experimental Raman profiles and calculated smeared PDOS; (ii) the consistent explanation

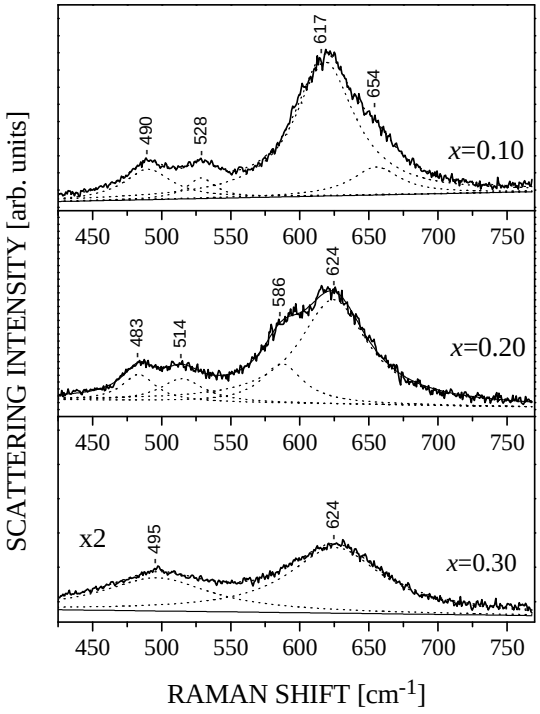

FIG. 8: Evolution of the HV spectrum between $x = 0.10$ and $x = 0.30$.

of the similarities between the Raman spectra of manganites with different average structure (orthorhombic or rhombohedral); (iii) the strong reduction or disappearance of the broad bands below the insulator-to-metal transition in the CMR materials.

Our results support the assumption for dominant role of Jahn-Teller-disorder-induced bands in the Raman spectra of heavily doped orthorhombic manganites. Indeed, the Raman spectrum of undoped $YMnO_3$ is well understood and the A_g line at 519 cm^{-1} and the B_{2g} line at 617 cm^{-1} correspond to the highest A_g and B_{2g} modes, respectively.[10] Therefore, the relatively weak band at 653-658 cm^{-1}, observed in the HH and HV spectra of $YMnO_3$, cannot be a proper Raman mode for the *Pnma* structure, but is rather due to contributions from zone-boundary phonons. This is consistent with lattice dynamical calculations, which predict for both $YMnO_3$ and $LaMnO_3$ the strongest PDOS peak close to this frequency.[18] This structure and another one near 490 cm^{-1}, where a PDOS maximum is also predicted, grow in relative weight with increasing x and become dominant at $x = 0.30$, while the lines related to Γ-point Raman modes, involving mainly oxygen motions are diminishing. This is exactly what one expects upon loss of translation symmetry with increasing oxygen

disorder. It is worth noting that the cationic sublattice also exhibits increasing disorder at higher x, indicated by noticeable broadening of the x-ray diffraction patterns for $x = 0.30$ and $x = 0.50$ (Fig.1). The x-ray patterns gain their intensities mainly from the Y, Ca and Mn atoms and to a lesser extent from the light oxygen atoms, which justifies such conclusion.

IV. CONCLUSIONS

We have successfully prepared orthorhombic $Y_{1-x}Ca_xMnO_3$ in a wide doping range between $x = 0$ and $x = 0.5$ using high-pressure synthesis. Between $x = 0$ and $x = 0.25$ the orthorhombic structure was stabilized as a metastable phase. The lattice parameters change gradually with x over the whole doping range. The Ca doping increases the conductivity, but its temperature dependence remains semiconducting for all x. The magnetic susceptibility for $x \leq 0.3$ exhibits the typical paramagnetic Curie dependence at high temperatures (> 80 K). The paramagnetic Curie temperature is negative for small x, crosses zero at $x \approx 0.08$ and becomes positive at larger x. This is interpreted as a gradual change of the magnetic correlations from antiferromagnetic superexchange ($x < 0.08$) to ferromagnetic double exchange interactions ($x > 0.08$) due to the replacement of Mn^{3+} with Mn^{4+} with increasing Ca doping. The evolution with x of the Raman spectra provide strong indications for increasing disorder of the oxygen sublattice for $x \geq 0.10$, presumably due to quasistatic and/or dynamic Jahn-Teller distortions. As a consequence of the loss of translational symmetry and activation of otherwise forbidden vibrations, the relatively broad bands in the Raman spectra for high substitution levels reflect rather the phonon density of states than the Raman allowed zone center phonons.

Acknowledgments

This work is supported in part by the state of Texas through the Texas Center for Superconductivity and Advanced Materials, by NSF grant no. DMR-9804325, the T.L.L. Temple Foundation, the J. J. and R. Moores Endowment, and at LBNL by the Director, Office of Energy Research, Office of Basic Energy Sciences, Division of Materials Sciences

of the US Department of Energy under contract no. DE-AC03-76SF00098.

---

[1] C. Moure, M. Villegas, J. F. Fernandez, J. Tartaj, P. Duran, Journal of Material Science **34**, 2565 (1999).

[2] A. Waintal and J. Chenavas, C. R. Acad. Sci. Ser.B **264**, 168 (1967).

[3] J. M. D. Coey, M. Viret, and S. von Molnár, Advances in Physics **48**, 167 (1999)(and references therein).

[4] H. W. Brinks, H. Fjellvag, and A. Kjekshus, J. Solid State Chem. **129**, 334 (1997).

[5] E. Pollert, S. Krupicka, E. Kuzmicova, J. Phys. Chem. Solids **43**, 1137 (1982)

[6] R. Mathieu, P. Nordblad, D. N. H. Nam, N. X. Phuc, N. V. Khiem, Phys. Rev. B **63**, 174405 (2001)

[7] Ch. Laberty, A. Navrotsky, C. N. R. Rao, P. Alphonse, J. Solid State Chem. **145**, 77 (1999)

[8] A. Munoz, J. A. Alonso, M. T. Casais, M. J. Martinez-Lope, J. L. Martinez, and M. T. Fernandez-Diaz, J. Phys.: Condens. Matter **14**, 3285 (2002).

[9] V. E. Wood, A. E. Austin, E. W. Collings, and K. C. Brog, J. Phys. Chem. Solids **34**, 859 (1973).

[10] M. N. Iliev, M. V. Abrashev, H. -G. Lee, V. N. Popov, Y. Y. Sun, C. Thomsen, R. L. Meng, and C. W. Chu, Phys. Rev. B **57**, 2872 (1998).

[11] V. B. Podobedov, A. Weber, D. B. Romero, J. P.Rice, and H. D. Drew, Solid State Commum. **105**, 589 (1998); Phys. Rev. B **58**, 43 (1998).

[12] S. Yoon, H. L. Liu, G. Schollerer, S. L. Cooper, P. D. Han, D. A. Payne, S.-W. Cheong, and Z. Fisk, Phys. Rev. B **58**, 2795 (1998).

[13] E. Granado, N. O. Moreno, A. Garcia, J. A. Sanjurjo, C. Rettori, I. Torriani, S. B. Oseroff, J. J. Neumeier, K. J. McClellan, S.-W. Cheong, and Y. Tokura, Phys. Rev. B **58**, 11 435 (1998).

[14] M. V. Abrashev, V. G. Ivanov, M. N. Iliev, R. A. Chakalov, R. I. Chakalova, and C. Thomsen, Phys. Status Solidi B **215**, 631 (1999).

[15] E. Liarokapis, Th. Leventouri, D. Lampakis, D. Palles, J. J. Neumeier, and D. H. Goodwin, Phys. Rev. B **60**, 12 758 (1999).

[16] P. Björnsson, M. Rübhausen, J. Bäckström, M. Käll, S. Eriksson, J. Eriksen, and L. Börjesson, Phys. Rev. B **61**, 1193 (2000).

[17] M. N. Iliev, A. P. Litvinchuk, M. V. Abrashev, V. G. Ivanov, H. G. Lee, W. H. McCarrol, M. Greenblatt, R. L. Meng, and C. W. Chu, Physica C **341-348**, 2257 (2000).

[18] M. N. Iliev, M. V. Abrashev, V. N. Popov, and V. G. Hadjiev, Phys. Rev. B **67**, 212301 (2003).